Enhancement of Local Piezoresponse in Polymer Ferroelectrics *via* Nanoscale Control of Microstructure

Yoon-Young Choi,[†] Pankaj Sharma,[‡] Charudatta Phatak,[†] David J. Gosztola,[§] Yunya Liu,[∥] Joonseok Lee,[§] Byeongdu Lee,[⊥] Jiangyu Li,[#] Alexei Gruverman,[‡] Stephen Ducharme,[‡] and Seungbum Hong*[,†]

[†]Materials Science Division, Argonne National Laboratory, Argonne, Illinois 60439, United States, [‡]Department of Physics and Astronomy, Nebraska Center for Materials and Nanoscience, University of Nebraska, Lincoln, Nebraska 68588, United States, [§]Center for Nanoscale Materials, Argonne National Laboratory, Argonne, Illinois 60439, United States, [∥]School of Materials Science and Engineering, Xiangtan University, Hunan 411105, People's Republic of China, [⊥]X-ray Sciences Division, Argonne National Laboratory, Argonne, Illinois 60439, United States, and [#]Department of Mechanical Engineering, University of Washington, Seattle, Washington 98195, United States

ABSTRACT Polymer ferroelectrics are flexible and lightweight electromechanical materials that are widely studied due to their potential application as sensors, actuators, and energy harvesters. However, one of the biggest challenges is their low piezoelectric coefficient. Here, we report a mechanical annealing effect based on local pressure induced by a nanoscale tip that enhances the local piezoresponse. This process can control the nanoscale material properties over a microscale area at room temperature. We attribute this improvement to the formation and growth of β-phase extended chain crystals *via* sliding diffusion and crystal alignment along the scan axis under high mechanical stress. We believe that this technique can be useful for local enhancement of piezoresponse in ferroelectric polymer thin films.

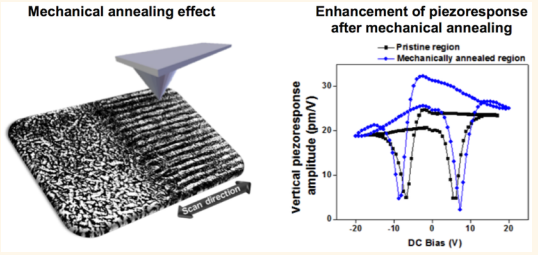

KEYWORDS: mechanical annealing effect · ferroelectric polymers · P(VDF-TrFE) · piezoresponse hysteresis loops

As flexible smart devices are being developed, nowadays, there is an increasing demand for using organic ferroelectric polymers as the functional components in such devices. The ferroelectric polymer of poly(vinylidene fluoride) (PVDF) and its copolymer poly(vinylidene fluoride-*co*-trifluoroethylene) (P(VDF-TrFE)) are widely used as ultrasonic transducers,[1,2] piezoelectric sensors,[3] electromechanical actuators,[2,3] and energy harvesters,[4] due to their relatively large remnant polarization,[5] high piezoelectric activity,[6] and the possibility of being easily integrated onto flexible substrates at low processing temperatures.[7]

However, one of the biggest deficiencies of polymer ferroelectric materials is their low piezoelectric coefficient (d_{33}), which is determined by the normal component of the local polarization,[8] which is, in turn, related to the crystallinity of the materials and the degree of alignment of the dipoles along the surface normal direction.[9] Therefore, there have been many efforts to enhance the intrinsic material properties of ferroelectric polymers using, for example, electrospinning,[10] nanoimprint lithography,[7] and mechanical shearing/drawing.[2,11,12]

Electrospinning can induce a phase transformation from nonpolar α-phase to polar β-phase in PVDF or P(VDF-TrFE) nanofibers *via* uniaxial stretching and electrical poling.[10,13] Nanoimprint lithography (NIL), which creates PVDF or P(VDF-TrFE) nanostructures by the mechanical deformation using a hard mold, can achieve crystal ordering by the confinement effects.[7,14,15] Large-scale control of molecular and microstructural orientation in P(VDF-TrFE) films was realized using the static mechanical shearing during melt and recrystallization process.[11,12] Mechanical drawing can control the macroscopic orientation of the thick PVDF film in the form of a freestanding structure over a large area while inducing the phase transition from nonpolar to polar phase at about 90 °C.[2,16]

* Address correspondence to hong@anl.gov.

Received for review November 25, 2014 and accepted February 3, 2015.

Published online February 03, 2015
10.1021/nn5067232

Although all these methods have led to improvement in either the ferroelectric polarization or piezoelectric coefficient, until now, there has been no appropriate method for enhancing piezoelectric properties of ferroelectric polymer films thinner than 100 nm. As ferroelectric polymers have high coercive fields of about 50 MV m^{-1}, thin films are required to reduce the switching voltage.[5,7] However, they suffer from the degradation of piezoelectric properties due to a reduction in crystallinity.[17,18]

Here, we present a novel technique that improves piezoelectric properties of thin P(VDF-TrFE) films by using local mechanical stress at room temperature. This process, termed "mechanical annealing", can control the material properties over a selected area in the films through sequential spatial integration of local interactions using a nanoscale tip. It should be noted that our work is different from the previous work reported by Kimura *et al.*[19−22] in the aspect of the temperature−pressure space and the structure−property relationship in terms of piezoelectric coefficient. We applied a local stress larger than the yield strength at room temperature and investigated the accompanying change in the piezoelectric properties, whereas they used much lower stress at elevated temperature and room temperature without detailed characterization of the piezoresponse hysteresis loop. In addition, we investigated the mechanism behind the increase in piezoelectric properties by systematically analyzing the change of molecular alignment and chain conformation and the change in the vertical and lateral polarization images using piezoresponse force microscopy (PFM).

RESULTS AND DISCUSSION

To investigate the relationship between the mechanical force and the material properties of the P(VDF-TrFE) thin films, we applied a mechanical force ranging from 0.6 to 1.4 μN to the film at room temperature by pressing the SPM tip against the sample surface during the scanning process as shown in Figure 1a.

In Figure 1b, SEM images show both pristine and mechanically annealed regions in P(VDF-TrFE) films. The surface morphology was irreversibly deformed under high mechanical stress ranging from 0.6 μN (212 MPa) to 1.4 μN (495 MPa), which is expected, as the applied stress is larger than the yield stress of 20−30 MPa.[23] Furthermore, the randomly oriented crystals in the pristine region became well aligned with the fast scan direction after the mechanical annealing, resulting in stripe domains as shown in Figure 1c. In addition, dark lines were formed between the annealed rows. We applied the mechanical force with a 30 nm radius tip during 64 line scans that were spaced 78 nm apart from each other. This value (*i.e.*, 78 nm) is in the range of measured values of line widths from SEM images (Figure 1c and d). Therefore, we think that the dark lines are the trajectories formed by the tip and aligned with the center of the tip, which was in contact with the surface.

Figure 1e shows the dependence of the surface roughness on the applied force. The root-mean-square (rms) surface roughness increased from 2.0 nm to 10.7 nm with the increasing mechanical force. The change of the surface roughness might be due to the wear of the film by the SPM tip during the scanning process under high mechanical stress. In addition, we believe that when the mechanical force increases, the protrusion of the film increases proportionally to the mechanical force due to the increase of the wear depth as the mechanical force increases.[24] The increase in the roughness is detrimental to many applications,[25] and we plan to explore additional means such as a post-annealing process to reduce the overall roughness. However, it should be noted that surface roughening can be useful in some cases where we want to increase the effective surface/volume ratio, as in the case of, for example, tribo-energy harvesting,[26] catalysis,[27,28] and electron emission.[29,30]

Furthermore, to elucidate the changes in the surface morphology distinctly, we obtained the cross-sectional transmission electron microscopy (TEM) image (see Figure 1f) covering both the pristine and the neighboring mechanically annealed region. After the mechanical annealing, the sample was prepared for TEM imaging by overcoating with a protective layer of gold, followed by focused ion beam (FIB) milling to cut (in the direction perpendicular to the fast scan direction in the mechanically annealed region) the sample suitably for cross-sectional imaging of the neighboring pristine and mechanically annealed regions. Although the interface between the pristine and the mechanically annealed regions shows a thinner part than other regions, we did not find any sign of significant damage in the films or delamination for a mechanical force of 1.0 μN (350 MPa) in the mechanically annealed regions. In addition, we clearly see that the surface roughness increased in the mechanically annealed region.

We measured the vertical and lateral piezoresponse hysteresis loops with a loading force of 125 nN using a dual ac resonance tracking (DART) mode of PFM[31] in both pristine and mechanically annealed regions, which were scanned with a mechanical force of 1.0 μN before the loop measurement, to investigate the effects of mechanical force on the piezoelectric properties of the P(VDF-TrFE) thin films. As shown in Figure 2b, the average remanent vertical piezoresponse amplitude increased from 21.9 $\pm$ 3.3 pm/V to 28 $\pm$ 6.9 pm/V and the coercive voltage (V_c) for vertical piezoresponse amplitude−voltage butterfly loops increased from 6.2 $\pm$ 0.5 V to 7.7 $\pm$ 0.2 V in the mechanically annealed region. The average remanent lateral piezoresponse amplitude also increased significantly from 0.8 $\pm$ 0.2 (au)

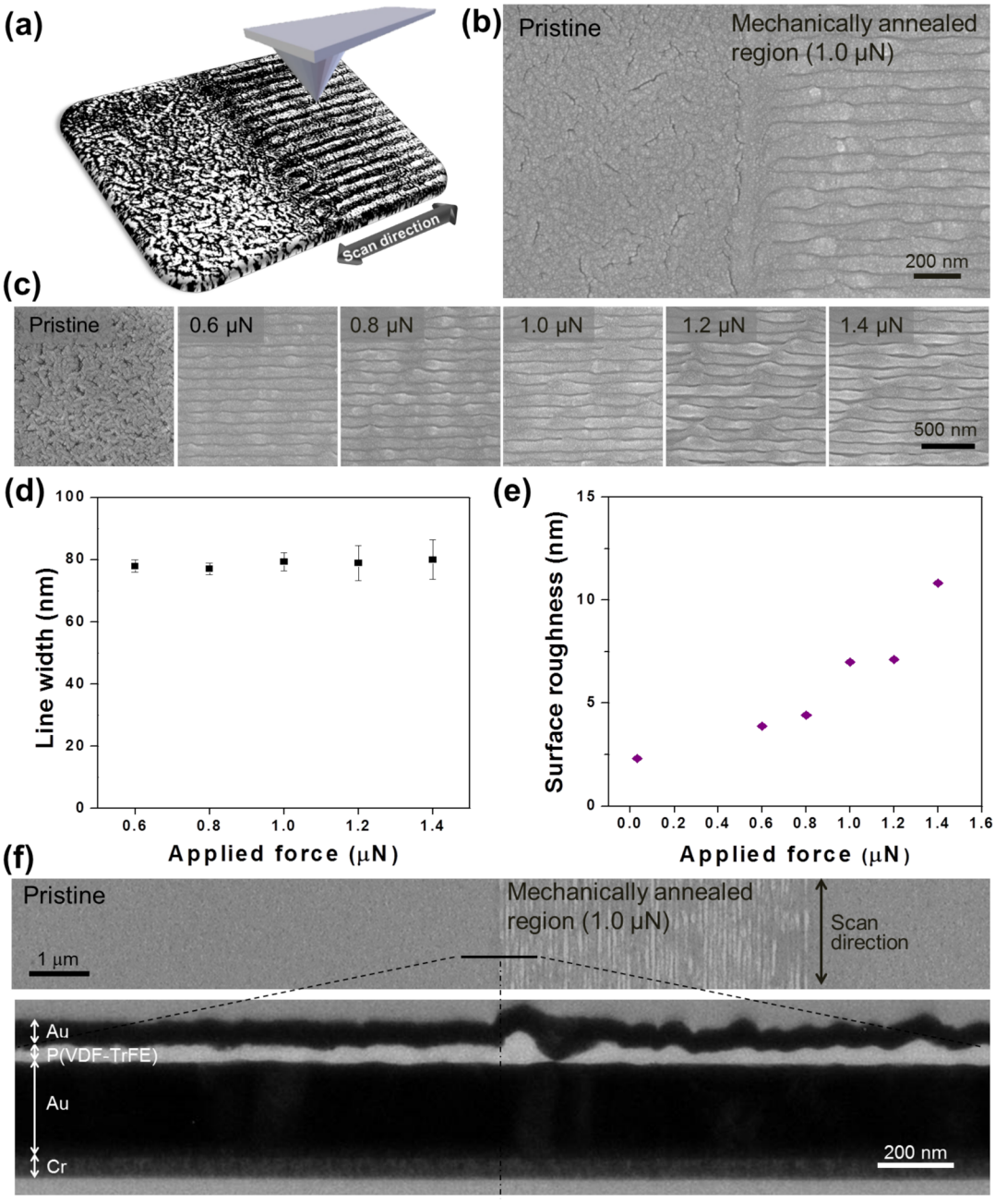

Figure 1. Surface morphology of a P(VDF-TrFE) thin film before and after mechanical annealing. (a) Schematic illustration of mechanical annealing on a P(VDF-TrFE) thin film using an SPM tip. (b) SEM image of the P(VDF-TrFE) thin film in pristine and mechanically annealed regions. (c–e) SEM images, measured line width, and surface roughness of the film as a function of mechanical force from 0.6 to 1.4 μN. (f) Cross sectional TEM image of the film in pristine and mechanically annealed regions.

to 1.7 ± 0.5 (au), and the coercive voltage (V_c) for lateral piezoresponse amplitude–voltage butterfly loops increased from 7.8 ± 1.4 V to 8.7 ± 0.8 V in the mechanically annealed region (see Figure 2d). The vertical and lateral piezoresponse amplitudes measured after the mechanical annealing were 28% and 102.4% higher than the pristine film in this study.

It should be noted that the observed lateral piezoresponse amplitude–voltage butterfly loops contain a component that is not usually observed in lateral piezoresponse loops induced by domain switching.[32] The possible scenario that can account for the small loops observed at the end of the loop is the anomalous contribution of (potentially charged) domain walls to the lateral piezoresponse, which upon reaching the maximum field disappear, as there are no more domain walls.[33]

In order to explore the changes in domain structure and the vector piezoresponse induced by the structural modification, we conducted vertical and lateral PFM imaging in both pristine and mechanically annealed regions. We scanned the pristine region over 1 μm × 1 μm area with an applied force of 0.03 μN to the tip,

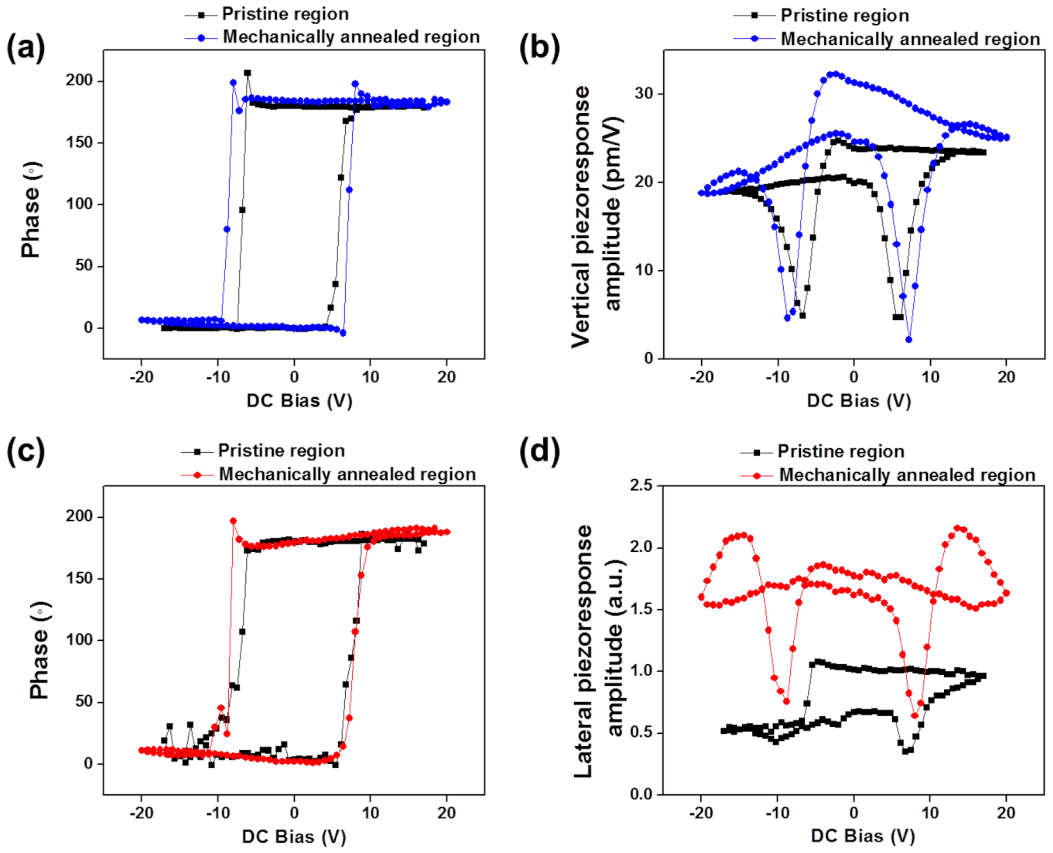

Figure 2. Vertical and lateral phase−voltage hysteresis loops (a, c) and amplitude−voltage butterfly loops (b, d). Vertical (a, b) and lateral (c, d) phase−voltage hysteresis loops and amplitude−voltage butterfly loops obtained from pristine (black squares) and mechanically annealed regions (blue circles for vertical and red circles for lateral phase−voltage hysteresis loops and amplitude−voltage butterfly loops).

as shown in Figure 3a and b. Then we scanned the mechanically annealed region using the same condition as above, which was formed by scanning the tip with a loading force of 1.0 μN over the pristine region as shown in Figure 3c and d.

Figure 3a shows granular-type domains with a random distribution of positive (up) and negative (down) piezoresponse vectors. However, in the mechanically annealed region, the randomly oriented domains changed their shapes to elongated stripe domains with downward vertical piezoresponse vectors, which match with the surface morphology of the mechanically annealed regions. In Figure S3, we applied a mechanical force ranging from 0.6 to 1.0 μN to the tip and obtained PFM images with an applied force of 0.03 μN to the tip in both pristine and mechanically annealed regions. Here we also confirmed that the randomly oriented vertical polarization vectors aligned along a downward direction and the vertical piezoresponse amplitude increased as we increased the mechanical force (Figure S3).

On the basis of lateral PFM images at a sample rotation angle of both 0° (Figure 3b and d) and 90° (see Figure S2 in the Supporting Information), we can confirm the formation of stripe domains in the mechanically annealed regions. In addition, randomly oriented lateral piezoresponse vectors in pristine regions became more uniform and were mostly aligned toward the perpendicular direction to the long axis of the stripe domains in the mechanically annealed regions based on Figure 3d and Figure S2 in the Supporting Information.

To understand the structural changes in the mechanically annealed region, we measured the Raman spectra of both pristine and mechanically annealed regions in the wavenumber range of 700−1500 cm^{-1} using micro-Raman spectroscopy. The band at 805 cm^{-1} can be assigned either to the crystalline α-phase, which consists of alternating trans−gauche conformations,[34] or the alternating trans−gauche conformations. The bands at 848 and 1292 cm^{-1} are assigned to the symmetric CF_2 stretching mode in the crystalline β-phase, possessing short and long trans sequences, respectively.[34,35] The band at 1430 cm^{-1} represents the CH_2 deformation mode of the VDF unit and gives a similar band for all crystalline forms.[36−38] The band at around 1350 cm^{-1} is unknown from the literature of Raman spectra on ferroelectric polymers. However, this band has been detected as a very weak band in FTIR (Fourier transform infrared) spectroscopy, and it represents a mixture of pure crystalline phase and disordered phase.[39]

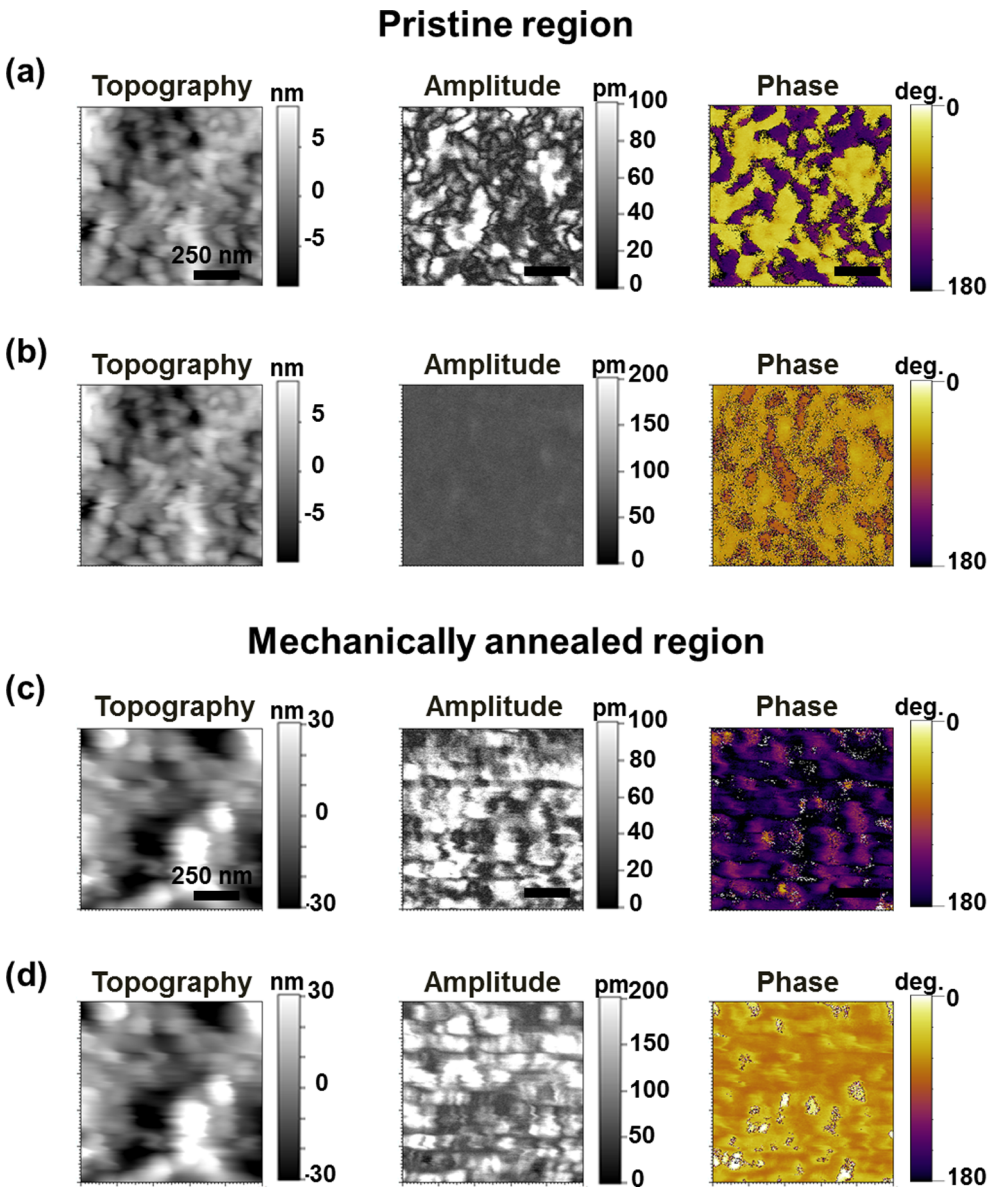

Figure 3. Vertical and lateral PFM images. (a–d) Topography, vertical (a, c) and lateral (b, d) piezoresponse amplitude and phase images of pristine (a, b) and mechanically annealed region (c, d) with a mechanical force of 1.0 μN.

As shown in Figure 4a, the bands at 848 and 1292 cm^{-1} related to the crystalline β-phase were observed in the pristine region. The band at 848 cm^{-1} decreased while the band at 1292 cm^{-1} increased in their intensities as the applied force increased. In the meantime, a new band at 805 cm^{-1} was observed when the mechanical force was larger than 0.8 μN, indicative of a critical force between 0.7 μN (247 MPa) and 0.8 μN (283 MPa) to form the trans–gauche conformations in the mechanically annealed region. On the basis of our finding from grazing incidence wide-angle X-ray scattering (GIWAXS) in Figure S6, we observed only the crystalline β-phase, which is oriented along the (200) or (110) planes where the *c*-axis is aligned parallel to the substrate without α-phase in both pristine and mechanically annealed regions (see Figure S5–7 in the Supporting Information). Therefore, we conclude that this band comes from the formation of trans–gauche conformations or defects under high mechanical stress.

In order to map the conformational and structural changes over the whole area of both the pristine and mechanically annealed regions, we measured the Raman spectra at each point on a 22 $\times$ 13 grid spanning an area of 33 μm $\times$ 19.5 μm, which covered the rectangular mechanically annealed region of 20 μm $\times$ 10 μm in the center and the pristine region around it (Figure 4b-1). We mapped the intensity of the Raman bands at 805, 848, and 1292 cm^{-1} over an area of 33 μm by 19.5 μm, which correspond to red, yellow, and green images, respectively, in Figure 4b. We found that the intensity of the bands at 805 and 1292 cm^{-1} increased and that of the band at 848 cm^{-1} decreased

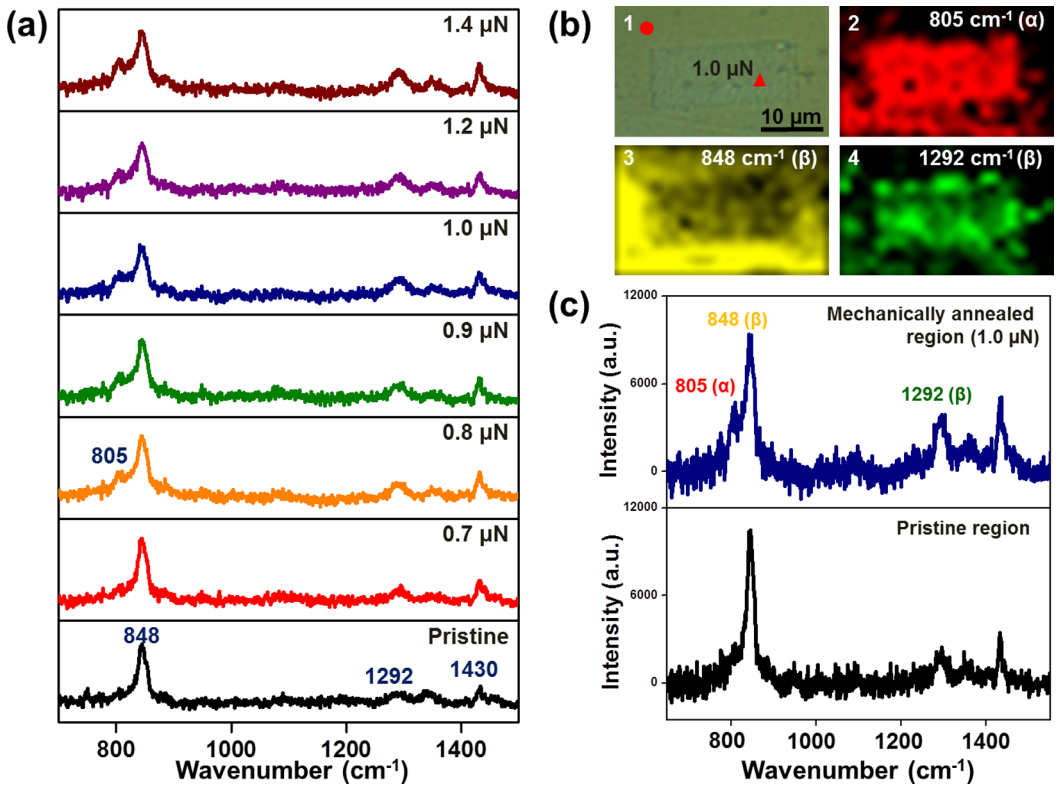

Figure 4. Raman spectra and mapping images of the P(VDF-TrFE) film before and after mechanical annealing. (a) Raman spectra of pristine and mechanically annealed regions as a function of mechanical force from 0.6 to 1.4 μN. (b) Optical microscope image (b-1), Raman mapping images at 805 (b-2), 848 (b-3), and 1294 cm^{-1} (b-4), and (c) Raman spectra measured at the circle-marked position (pristine region) of image b-1 and at the triangle-marked position of image b-1 (mechanically annealed region).

in the mechanically annealed region, which agrees with the observation made from Figure 4a. Figure 4c shows the representative Raman spectra for both pristine (circle-marked position) and mechanically annealed (triangle-marked position) regions, which were selected from the sets of the spectra used for Raman mapping in Figure 4b.

Here, we suggest a model that explains both the structure and property changes induced by the mechanical annealing. We believe that the main mechanism is the formation, growth, and reorientation of the lamellar crystals resulting from the sliding diffusion of molecular segments along the chain axis under high mechanical stress (Figure 5).

First, it is known that under high mechanical pressure and high temperature the polymer chains form β-extended chain crystals (β-ECCs) through the sliding diffusion.[40−43] We assume that the sliding motion of the tip with high pressure creates a similar environment underneath the tip, where both the pressure and temperature are comparable to the condition under which the β-ECCs form through the sliding diffusion.

Therefore, we think that the formation and growth of the β-phase extended chain crystals from a crystalline β-phase were increased when the tip moved under a local tip-induced pressure of 350 MPa. We hypothesize that the local pressure facilitates the kinetics of crystallization of the β-phase with long trans sequences from the original β-phase via enhanced sliding diffusion.

Second, the sliding motion of the tip under high pressure also creates regions that experience a high shear stress up to 150 MPa, which is calculated by multiplying the normal stress and the friction coefficient.[44] The high shear stress around 150 MPa can lead to a decrease in viscosity due to the shear thinning effect.[45] When the viscosity decreases, the defect density increases as a result of the increase in the disorder of the molecular chains.[45] This will, in turn, increase the interchain separation and result in a shorter coherence length of the crystalline regions, in which conformations with trans (T) and gauche (G) bonds are energetically favored.[45−47] As a result, the G bonds will form more easily in the all-trans conformations with a short trans sequence.

On the basis of the model described above, the increase of peak intensity of Raman scattering at 1292 cm^{-1} results from the formation and growth of the β-ECCs under high mechanical stress. Furthermore, the increase in peak intensity at 805 cm^{-1} and the decrease in peak intensity at 848 cm^{-1} result from the nucleation of G bonds in all-trans conformations, which consist of short trans sequences. Although the increase in trans−gauche conformations or defects in the β-phase with short trans sequences results in the decrease of the piezoresponse, we think the an increase in β-phase with

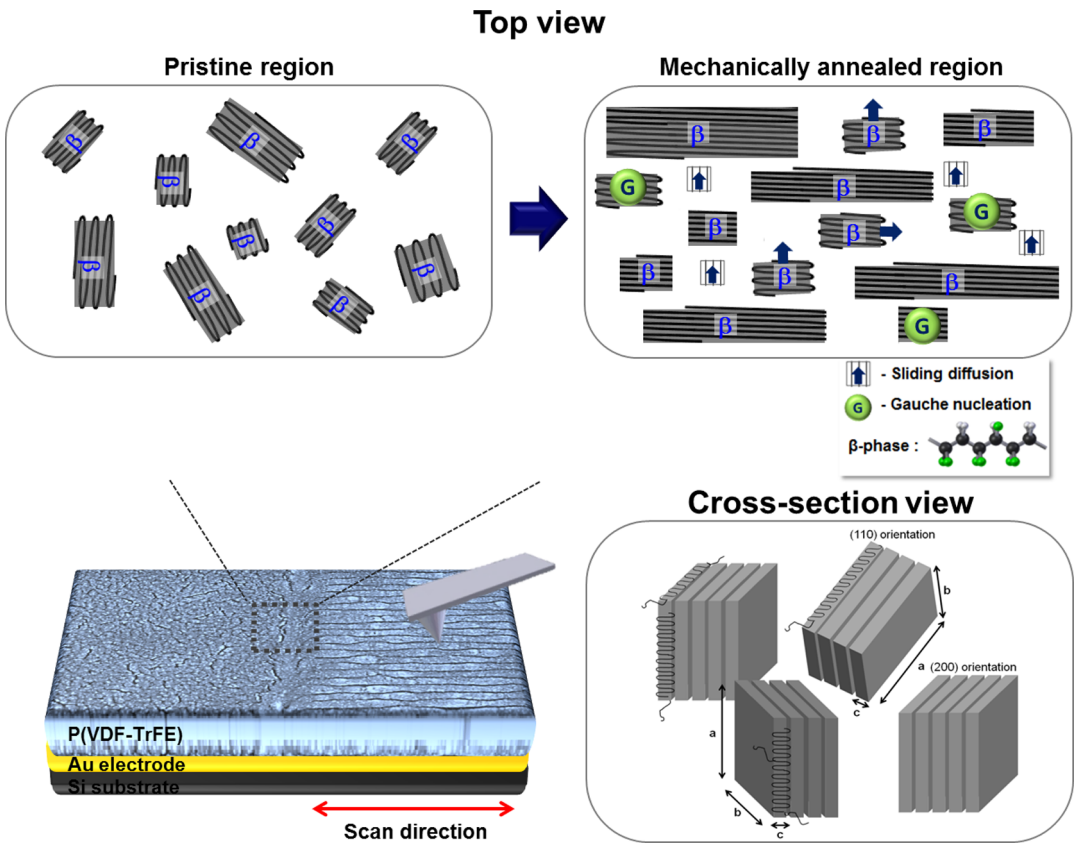

Figure 5. Schematic illustration of a hypothetical mechanism with top and cross-section views. The top illustration shows the procedure of the mechanical annealing, where the randomly oriented β-phase crystallites form a β-phase with long trans sequences aligned along the scan direction resulting from sliding diffusion. In addition, G bonds easily form in the all-trans conformations, which consist of short trans sequences. The cross-section illustration shows the β-phase oriented along either (200) or (110) planes, where the *c*-axis is aligned parallel to the substrate in both pristine and mechanically annealed regions.

long trans sequences counteracted the negative impact of the defects and played the dominant role in the increase of the piezoresponse after mechanical annealing.

Finally, when the film is yielded due to the high tensile stress induced by the tip, the crystal structure can be disrupted by the "slip", which occurs within the individual lamellar crystals, leading to a molecular reorientation along the tensile axis.[48] It is worth noting that although the tip is exerting compressive stress beneath and at the moving front, the trailing part and the vicinity will experience tensile stress, which will contribute to the slip. Therefore, the lamellar crystals will be aligned along the scanning direction, which, along with the formation of β-ECCs, accompanies the formation of the long stripe domains with the piezoresponse vector pointing perpendicular to the scan axis. We think that the formation of well-aligned long stripe domains after mechanical annealing also contributes to enhancement of the piezoresponse because it may accompany the reduction of imperfections and defects in the crystalline β-phase with long trans sequences.[49,50]

With the structural change in terms of morphology, phase, and domain configuration understood by the model in Figure 5, we extend the model to explain the improvement in the piezoresponse property shown in Figure 2 using a nonlinear phenomenological theory of ferroelectrics. It should be noted that the mechanical clamping effect by the tip when applying pressure to the tip is not considered in the model,[51−53] which limits the interpretation to the case where the increase in the remnant piezoresponse can be measured at ambient pressure if the polarization rotation is nonvolatile after the release of the pressure. On the basis of our SEM, PFM, and hysteresis results obtained in atmospheric conditions after mechanical annealing, we confirmed that the polarization rotation induced by the pressure was nonvolatile even after the release of the pressure. This indicates that the structural changes induced by plastic deformation in the mechanically annealed region can be coupled with the rotation of polarization.

In addition, our model does not include the microstructure changes and phase transitions of P(VDF-TrFE) induced by the local pressure, as nonlinear phenomenological theory is a macroscopic method. However, our model captures the macroscopic effect of mechanical stress on polarization, which can explain the rotation of polarization and increase in the remnant piezoresponse induced by the applied stress *via* the SPM tip.

The free energy of P(VDF-TrFE) can be expanded in terms of the polynomial of polarization P_i (i = 1, 2, 3)

and stress σ_I (I = 1, 2, ..., 6) given in Voigt notation and expressed as[54]

$$G = \frac{\alpha}{2}(P_1^2+P_3^2)+\frac{\beta}{4}(P_1^2+P_3^2)^2+\frac{\gamma_1}{6}(P_1^2+P_3^2)^3 + \frac{\gamma_2}{2}P_1^2(P_1^2-3P_3^2)^2-\frac{S_{11}}{2}(\sigma_1^2+\sigma_2^2+\sigma_3^2) - S_{12}(\sigma_1\sigma_2+\sigma_1\sigma_3+\sigma_2\sigma_3)-\frac{S_{44}}{2}(\sigma_4^2+\sigma_5^2+\sigma_6^2) - Q_{11}(\sigma_1P_1^2+\sigma_2P_2^2+\sigma_3P_3^2)-Q_{12}[\sigma_1(P_2^2+P_3^2) + \sigma_2(P_1^2+P_3^2)+\sigma_3(P_1^2+P_2^2)]-Q_{44}(\sigma_4P_2P_3 + \sigma_5P_1P_3+\sigma_6P_1P_2)-E_1P_1-E_2P_2-E_3P_3 \quad (1)$$

where α is a temperature-dependent function, β, γ_1, and γ_2 are constants, S_{IJ} is the elastic compliance constant measured at constant polarization, Q_{IJ} is the electrostrictive coefficient coupling the elastic and electric field in ferroelectrics, and the E_i is electric field.

The polarization can be determined by minimizing the free energy, and the corresponding piezoelectric coefficients can be evaluated accordingly, as detailed elsewhere.[55] It should be noted that the polarization vectors (P) and the piezoresponse vectors (U) have different amplitude ratios between out-of-plane (vertical) and in-plane (lateral) components and overall directions due to the dependence of both vertical and lateral piezoresponse vectors on various piezoelectric coefficients shown in eqs 2 and 3.

Before the mechanical force loading, P(VDF-TrFE) films are under a stress-free state. In this case, the minimization of free energy corresponds to the six possible polarization (P) variants coexisting, which agrees with the observation of a random distribution of positive (up) and negative (down) piezoresponse vectors (U) in the vertical PFM images (Figure 3a).

Considering the initial piezoresponse vectors of P(VDF-TrFE), being $U_3 < 0$ and $U_1 < 0$, and the polarities of U_3 and U_1 were the same as those of P_3 and P_1, the variation of polarization under the mechanical force is calculated, as shown in Figure S8a, which suggests that the polarization is rotated downward on increasing the out-of-plane component and decreasing the in-plane component.

The corresponding vertical (U_3) and lateral (U_1) piezoresponse can be evaluated using the following analytical expression:[56]

$$U_3 = V_Q\left[-\frac{1+4\nu}{8}(d_{31}+d_{32})-\frac{3}{4}d_{33}-\frac{1}{8}(d_{24}+d_{15})\right] \quad (2)$$

$$U_1 = V_Q\left[-\frac{13+4\nu}{32}d_{11}+\frac{1-12\nu}{32}d_{12}-\frac{1}{8}d_{13} - \frac{3}{8}d_{35}-\frac{7-4\nu}{32}d_{26}\right] \quad (3)$$

which was derived by Eliseev *et al.*[56] for general piezoelectric anisotropy under the assumption that P(VDF-TrFE) thin films are dielectrically isotropic. Note that V_Q is the external potential applied to the SPM tip, ν is the Poisson ratio, and piezoelectric coefficients can be calculated using the nonlinear phenomenological theory.

The calculated values of the vertical ($U_3(\sigma)$) and lateral ($U_1(\sigma)$) piezoresponses in the stressed regions of the film, normalized by the values measured in the unstressed regions, are shown in Figure S8b, which suggest that both vertical and lateral piezoresponses can be enhanced under the mechanical force. It should be noted that $U_3(\sigma)$ and $U_1(\sigma)$ induced by σ will retain their values even after the removal of σ, indicative of either metastable or stable transition by the stress. This is in a good qualitative agreement with our experimental observation of enhancement of both vertical and lateral remanent piezoresponses as shown in Figure 2 and the schematic illustration of the piezoresponse vector configuration after mechanical annealing, as shown in Figure S9, constructed based on the vertical and lateral PFM images in the selected area shown in Figure 3.

CONCLUSIONS

In conclusion, we report a mechanical annealing effect in the ferroelectric polymers induced by the SPM tip-generated stress, which results in enhancement of the local piezoelectric response. Piezoresponse force microscopy imaging and Raman spectroscopy show that the mechanical annealing increases the volume fraction of the ferroelectric β-phase with a long chain sequence and aligns the in-plane component of polarization toward the direction perpendicular to the scan direction. We believe that this new technique can be used for enhancement of molecular alignment and piezoelectric property. In order to apply "mechanical annealing" to large-scale production of a high-performance piezoelectric device, we are currently developing techniques for scale-up using either a roller with multiple sharp tips or a macroscale razor blade with nanoscale sharpness.

MATERIALS AND METHODS

Materials Preparation. We dissolved 0.01 g of P(VDF-TrFE) powder (75/25 mol %, MSI Sensors Inc.) in methyl ethyl ketone. The solution was filtered by 0.22 μm pore size PTFE membrane syringe filters, and then the filtered solution was spin-coated onto the Au/Cr/SiO_2/Si substrate at 1500 rpm for 10 s. The spin-coated film was subsequently annealed at 130 °C for 1 h on a hot plate. The resulting thickness of the P(VDF-TrFE) film was about 50 nm. The thickness was measured by cross-section TEM (FEI Tecnai F20ST).

Mechanical Annealing Using an SPM Tip. We applied mechanical force ranging from 0.6 to 1.4 μN to the film using atomic force microscopy (MFP-3D AFM, Asylum Research) with a Pt/Ir-coated tip (radius of 30 nm, PPP-EFM, Nanosensors) during 64 line scans with a scan rate of 1 Hz. Mechanical force was determined by multiplying the spring constant of the cantilever (2.2−3.4 N/m), the inverse optical lever sensitivity (40.6−58.1 nm/V), and the cantilever deflection signal (6−11 V).

Morphology Characterization. The change of the surface morphology was confirmed *via* field emission scanning electron microscopy (FESEM, JEOL JSM-7500). The change of the surface roughness was measured by AFM and cross-sectional TEM on both as-grown and mechanically annealed regions.

Piezoresponse Hysteresis Loop Measurement. The vertical and lateral piezoresponse hysteresis loops were measured by dual ac resonance tracking PFM (DART-PFM)[31] mode in both the pristine and the mechanically annealed regions. The loading force was around 125 nN. The local piezoresponse hysteresis loops were measured at three different arbitrary points for four times at each position. The vertical piezoresponse was calibrated using the inverse optical lever sensitivity obtained from the force−distance curve and adjusted by dividing the calibrated amplitude by the quality factor based on a simple harmonic oscillator model. The inverse optical lever sensitivity refers to the ratio of the absolute displacement of the tip to the output voltage of the photodiode sensor, and the force−distance curve refers to the plot of the photodiode voltage as a function of the z-actuator position that moves the tip up and down. It should be noted that DART-PFM oscillated the cantilever close to the resonance; hence the absolute phase can change from 0° to 180° depending on where we put the drive frequency. Therefore, while the phase difference between two opposite domains remains 180°, the absolute phase for each domain could deviate from either 0° or 180°. In addition, as the amplitude is enhanced by the resonance, we need to calibrate the amplitude by dividing it by the quality factor.[15]

PFM Imaging. The vertical and lateral PFM images were obtained with drive frequencies near the contact resonance for vertical and torsional motions of PFM cantilevers, which were 171.96 and 684.52 kHz, respectively. Using a microrotation stage (7R128, Altos Photonics), we rotated the sample by 90° increments and adjusted the scan angle by the same amount to map the same region of interest.

Raman Spectroscopy and Mapping. Raman spectra were recorded using a Raman microscope (Renishaw inVia) using 633 nm excitation from a HeNe laser in the range 500−1500 cm^{-1}. The sample was excited by 8 mW incident laser power, and scattered light was collected through a 50× objective lens (Leica, numerical aperture (NA) = 0.75) with 2 μm spot size. We measured the Raman spectra at each point on 22 × 13 grids over an area of 33 μm by 19.5 μm and mapped the intensity of Raman bands at 805, 848, 1292, and 1430 cm^{-1} over the entire region. Each data point resulted from averaging 10 integrations with an acquisition time of 20 s for each integration.

Grazing Incidence Small- and Wide-Angle X-ray scattering. A 50 nm thick P(VDF-TrFE) film coated on highly doped n-type silicon was prepared by the Langmuir−Blodgett technique and was annealed at 130 °C for 1 h. A mechanically annealed region of 1 mm long and 50 μm wide was prepared using an SPM tip. GISAXS and GIWAXS were measured at the beamline 12-ID-B at Advanced Photon Source, Argonne National Laboratory. A 14 keV X-ray beam was focused on a 50 × 10 μm^2 ($H \times V$) area at an incident angle of 0.12°. Pilatus2M and PerkinElmer XRD 1621 CN detectors were used for GISAXS and GIWAXS, respectively. The sample to detector distance for GISAXS was about 3.2 m, and that for GIWAXS was about 0.15 m.

Modeling. The effects of mechanical force on the polarization and PFM response were calculated using the nonlinear phenomenological theory of ferroelectrics.

Conflict of Interest: The authors declare no competing financial interest.

Acknowledgment. The authors gratefully acknowledge T. Wang for fabrication of Langmuir−Blodgett P(VDF-TrFE) films for X-ray measurement. The submitted manuscript was created by UChicago Argonne, LLC, Operator of Argonne National Laboratory ("Argonne"). Argonne, a U.S. Department of Energy Office of Science Laboratory, is operated under Contract No. DE-AC02-06CH11357. The U.S. Government retains for itself, and others acting on its behalf, a paid nonexclusive, irrevocable worldwide license in said article to reproduce, prepare derivative works, distribute copies to the public, and perform publicly and display publicly, by or on behalf of the Government. The works of Raman spectroscopy, SEM and TEM imaging, and GIWAXS were performed at the Center for Nanoscale Materials, Electron Microscopy Center and Advanced Photon Source, a U.S. Department of Energy, Office of Science, Office of Basic Energy Sciences User Facilities, under Contract DE-AC02-06CH11357. The research at the University of Nebraska−Lincoln (PFM characterization and sample fabrication by P. Sharma, A. Gruverman, and S. Ducharme) was supported by the National Science Foundation (NSF) through the Materials Research Science and Engineering Center (MRSEC) under Grant DMR-1420645. Y.Y.L. acknowledges the support of NSFC (11102175), and J.Li. acknowledges the support of the NSF (CMMI-1100339).

Supporting Information Available: Additional vertical and lateral phase−voltage hysteresis loops and amplitude−voltage butterfly loops, vertical and lateral PFM images, GISAXS and GIWAXS images, and normalized polarization components along vertical and lateral directions as a function of mechanical stress. This material is available free of charge *via* the Internet at http://pubs.acs.org.

REFERENCES AND NOTES

1. Platte, M. PVDF Ultrasonic Transducers. *Ferroelectrics* **1987**, *75*, 327–337.
2. Lovinger, A. J. Ferroelectric Polymers. *Science* **1983**, *220*, 1115–1121.
3. Li, M. Y.; Wondergem, H. J.; Spijkman, M. J.; Asadi, K.; Katsouras, I.; Blom, P. W. M.; de Leeuw, D. M. Revisiting the Delta-Phase of Poly(vinylidene fluoride) for Solution-Processed Ferroelectric Thin Films. *Nat. Mater.* **2013**, *12*, 433–438.
4. Chang, C.; Tran, V. H.; Wang, J.; Fuh, Y. K.; Lin, L. Direct-Write Piezoelectric Polymeric Nanogenerator with High Energy Conversion Efficiency. *Nano Lett.* **2010**, *10*, 726–731.
5. Choi, Y.-Y.; Hong, J.; Leem, D.-S.; Park, M.; Song, H.; Sung, T.-H.; No, K. Spin-Coated Ultrathin Poly(vinylidene fluoride-co-trifluoroethylene) Films for Flexible and Transparent Electronics. *J. Mater. Chem.* **2011**, *21*, 5057–5061.
6. Sun, C.-L.; Lam, K. H.; Chao, C.; Lau, S. T.; Chan, H. L. W.; Guo, S.; Zhao, X. Fabrication and Characterization of Ni/P(VDF-TrFE) Nanoscaled Coaxial Cables. *Appl. Phys. Lett.* **2007**, *90*, 253107.
7. Hu, Z. J.; Tian, M. W.; Nysten, B.; Jonas, A. M. Regular Arrays of Highly Ordered Ferroelectric Polymer Nanostructures for Non-Volatile Low-Voltage Memories. *Nat. Mater.* **2009**, *8*, 62–67.
8. Lu, H.; Liu, X.; Burton, J. D.; Bark, C. W.; Wang, Y.; Zhang, Y.; Kim, D. J.; Stamm, A.; Lukashev, P.; Felker, D. A.; *et al.* Enhancement of Ferroelectric Polarization Stability by Interface Engineering. *Adv. Mater.* **2012**, *24*, 1209–1216.
9. Ohigashi, H.; Hattori, T. Improvement of Piezoelectric Properties of Poly(vinylidene fluoride) and its Copolymers by Crystallization under High Pressures. *Ferroelectrics* **1995**, *171*, 11–32.
10. Andrew, J. S.; Clarke, D. R. Effect of Electrospinning on the Ferroelectric Phase Content of Polyvinylidene Difluoride Fibers. *Langmuir* **2008**, *24*, 670–672.
11. Jung, H. J.; Chang, J.; Park, Y. J.; Kang, S. J.; Lotz, B.; Huh, J.; Park, C. Shear-Induced Ordering of Ferroelectric Crystals in Spin-Coated Thin Poly(vinylidene fluoride-co-trifluoroethylene) Films. *Macromolecules* **2009**, *42*, 4148–4154.
12. Chang, J.; Jung, H. J.; Jeong, H.; Park, Y. J.; Sung, J.; Kang, S. J.; Jung, G. Y.; Sung, M. M.; Park, C. One-Step Micropatterning of Highly-Ordered Semi-Crystalline Poly(vinylidene fluoride-co-trifluoroethylene) Films by a Selective Shear and Detachment Process. *Org. Electron.* **2011**, *12*, 98–107.

13. Persano, L.; Dagdeviren, C.; Su, Y.; Zhang, Y.; Girardo, S.; Pisignano, D.; Huang, Y.; Rogers, J. A. High Performance Piezoelectric Devices Based on Aligned Arrays of Nanofibers of Poly(vinylidenefluoride-co-trifluoroethylene). *Nat. Commun.* **2013**, *4*, 1633.
14. Hu, Z. J.; Baralia, G.; Bayot, V.; Gohy, J. F.; Jonas, A. M. Nanoscale Control of Polymer Crystallization by Nanoimprint Lithography. *Nano Lett.* **2005**, *5*, 1738–1743.
15. Liu, Y. M.; Weiss, D. N.; Li, J. Y. Rapid Nanoimprinting and Excellent Piezoresponse of Polymeric Ferroelectric Nanostructures. *ACS Nano* **2010**, *4*, 83–90.
16. Lei, C. H.; Hu, B.; Xu, R. J.; Cai, Q.; Shi, W. Q. Influence of Room-Temperature-Stretching Technology on the Crystalline Morphology and Microstructure of PVDF Hard Elastic Film. *J. Appl. Polym. Sci.* **2014**, *131*, 40077.
17. Xia, F.; Xu, H.; Fang, F.; Razavi, B.; Cheng, Z. Y.; Lu, Y.; Xu, B.; Zhang, Q. M. Thickness Dependence of Ferroelectric Polarization Switching in Poly(vinylidene fluoride–trifluoroethylene) Spin Cast Films. *Appl. Phys. Lett.* **2001**, *78*, 1122–1124.
18. Zhang, Q. M.; Xu, H.; Fang, F.; Cheng, Z. Y.; Xia, F.; You, H. Critical Thickness of Crystallization and Discontinuous Change in Ferroelectric Behavior with Thickness in Ferroelectric Polymer Thin Films. *J. Appl. Phys.* **2001**, *89*, 2613–2616.
19. Kimura, K.; Kobayashi, K.; Yamada, H.; Horiuchi, T.; Ishida, K.; Matsushige, K. Orientation Control of Poly(vinylidenefluoride-trifluoroethylene) Crystals and Molecules Using Atomic Force Microscopy. *Appl. Phys. Lett.* **2003**, *82*, 4050–4052.
20. Kimura, K.; Kobayashi, K.; Yamada, H.; Horiuchi, T.; Ishida, K.; Matsushige, K. Orientation Control of Molecular Chains in Polymers Using Atomic Force Microscopy. *Jpn. J. Appl. Phys.* **2004**, *43*, 4575–4579.
21. Kimura, K.; Kobayashi, K.; Yamada, H.; Horiuchi, T.; Ishida, K.; Matsushige, K. Orientation Control of Ferroelectric Polymer Molecules Using Contact-Mode AFM. *Eur. Polym. J.* **2004**, *40*, 933–938.
22. Kimura, K.; Kobayashi, K.; Yamada, H.; Matsushige, K. Investigation of Molecular Chain Orientation Change of Polymer Crystals in Phase Transitions by Friction Anisotropy Measurement. *Langmuir* **2007**, *23*, 4740–4745.
23. Park, J.-M.; Kong, J.-W.; Kim, D.-S.; Yoon, D.-J. Nondestructive Damage Detection and Interfacial Evaluation of Single-Fibers/Epoxy Composites Using PZT, PVDF and P(VDF-TrFE) Copolymer Sensors. *Compos. Sci. Technol.* **2005**, *65*, 241–256.
24. Chung, K.-H.; Lee, Y.-H.; Kim, Y.-T.; Kim, D.-E.; Yoo, J.; Hong, S. Nano-Tribological Characteristics of PZT Thin Film Investigated by Atomic Force Microscopy. *Surf. Coat. Technol.* **2007**, *201*, 7983–7991.
25. Choi, S. H.; Bae, B. J.; Son, Y. H.; Lim, J. E.; Yoo, D. C.; Im, D. H.; Heo, J. E.; Nam, S. D.; Park, J. H.; Hong, C. K.; *et al*. Study of Electrical Properties of Flattened MOCVD PZT Film by CMP Process. *Integr. Ferroelectr.* **2005**, *75*, 215–223.
26. Wang, S.; Niu, S.; Yang, J.; Lin, L.; Wang, Z. L. Quantitative Measurements of Vibration Amplitude Using a Contact-Mode Freestanding Triboelectric Nanogenerator. *ACS Nano* **2014**, *8*, 12004–12013.
27. Garrity, K.; Kakekhani, A.; Kolpak, A.; Ismail-Beigi, S. Ferroelectric Surface Chemistry: First-Principles Study of the $PbTiO_3$ Surface. *Phys. Rev. B* **2013**, *88*, 045401.
28. Smith, M. A.; Zoelle, A.; Yang, Y.; Rioux, R. M.; Hamilton, N. G.; Amakawa, K.; Nielsen, P. K.; Trunschke, A. Surface Roughness Effects in the Catalytic Behavior of Vanadia Supported on SBA-15. *J. Catal.* **2014**, *312*, 170–178.
29. Mimura, H.; Miyajima, K.; Yokoo, K. Electron Emission from Porous Silicon Planar Emitters. *J. Vac. Sci. Technol. B* **2003**, *21*, 1612–1615.
30. Yaseen, M.; Lou, X.; Chen, X.; Ren, W.; Liu, Y.; Feng, Y.; Shi, P.; Wu, X. Strong Electron Emission from Antiferroelectric PLZT(2/95/5) Films. *Appl. Phys. Lett.* **2014**, *104*, 222913.
31. Rodriguez, B. J.; Callahan, C.; Kalinin, S. V.; Proksch, R. Dual-Frequency Resonance-Tracking Atomic Force Microscopy. *Nanotechnology* **2007**, *18*, 475504.
32. Kalinin, S. V.; Gruverman, A.; Bonnell, D. A. Quantitative Analysis of Nanoscale Switching in $SrBi_2Ta_2O_9$ Thin Films by Piezoresponse Force Microscopy. *Appl. Phys. Lett.* **2004**, *85*, 795.
33. Sluka, T.; Tagantsev, A. K.; Damjanovic, D.; Gureev, M.; Setter, N. Enhanced Electromechanical Response of Ferroelectrics Due to Charged Domain Walls. *Nat. Commun.* **2012**, *3*, 748.
34. Gil, H. A. C.; Faria, R. M.; Kawano, Y. Structural Modifications of Vinylidene Fluoride-Trifluoroethylene (70−30) Copolymer Induced by X-ray Irradiation. *Polym. Degrad. Stab.* **1998**, *61*, 265–273.
35. Tashiro, K. Annealing Effects on Ferroelectric Phase Transitional Behavior of Vinylidene Fluoride-Trifluoroethylene Copolymers: An Interpretation Based on the Concept of Domain and Trans-Gauche Conformational Disorder. *Ferroelectrics* **1995**, *171*, 145–162.
36. Boccaccio, T.; Bottino, A.; Capannelli, G.; Piaggio, P. Characterization of PVDF Membranes by Vibrational Spectroscopy. *J. Membr. Sci.* **2002**, *210*, 315–329.
37. Kobayashi, M.; Tashiro, K.; Tadokoro, H. Molecular Vibrations of 3 Crystal Forms of Poly(Vinylidene Fluoride). *Macromolecules* **1975**, *8*, 158–171.
38. Tashiro, K.; Kobayashi, M. Vibrational Spectroscopic Study of the Ferroelectric Phase-Transition in Vinylidene Fluoride Trifluoroethylene Copolymers: 1. Temperature-Dependence of the Raman-Spectra. *Polymer* **1988**, *29*, 426–436.
39. Kim, K. J.; Reynolds, N. M.; Hsu, S. L. Spectroscopic Analysis of the Crystalline and Amorphous Phases in a Vinylidene Fluoride Trifluoroethylene Copolymer. *Macromolecules* **1989**, *22*, 4395–4401.
40. Hattori, T.; Watanabe, T.; Akama, S.; Hikosaka, M.; Ohigashi, H. The High-Pressure Crystallization Behaviours and Piezoelectricity of Extended Chain Lamellar Crystals of Vinylidene Fluoride Trifluoroethylene Copolymers with High Molar Content of Vinylidene Fluoride. *Polymer* **1997**, *38*, 3505–3511.
41. Yee, W. A.; Nguyen, A. C.; Lee, P. S.; Kotaki, M.; Liu, Y.; Tan, B. T.; Mhaisalkar, S.; Lu, X. Stress-Induced Structural Changes in Electrospun Polyvinylidene Difluoride Nanofibers Collected Using a Modified Rotating Disk. *Polymer* **2008**, *49*, 4196–4203.
42. Koga, K.; Nakano, N.; Hattori, T.; Ohigashi, H. Crystallization, Field-Induced Phase Transformation, Thermally Induced Phase Transition, and Piezoelectric Activity in P(vinylidene fluoride-TrFE) Copolymers with High Molar Content of Vinylidene Fluoride. *J. Appl. Phys.* **1990**, *67*, 965–974.
43. Huang, S.; Yee, W. A.; Tjiu, W. C.; Liu, Y.; Kotaki, M.; Boey, Y. C. F.; Ma, J.; Liu, T.; Lu, X. Electrospinning of Polyvinylidene Difluoride with Carbon Nanotubes: Synergistic Effects of Extensional Force and Interfacial Interaction on Crystalline Structures. *Langmuir* **2008**, *24*, 13621–13626.
44. Gines, R.; Bergamini, A.; Christen, R.; Motavalli, M.; Ermanni, P. Frictional Behaviour of Polymer Films under Mechanical and Electrostatic Loads. *Smart Mater. Struct.* **2013**, *22*, 075023.
45. Su, H.; Strachan, A.; Goddard, W. Density Functional Theory and Molecular Dynamics Studies of the Energetics and Kinetics of Electroactive Polymers: PVDF and P(VDF-TrFE). *Phys. Rev. B* **2004**, *70*, 064101.
46. Bao, H. M.; Song, J. F.; Zhang, J.; Shen, Q. D.; Yang, C. Z.; Zhang, Q. M. Phase Transitions and Ferroelectric Relaxor Behavior in P(VDF-TrFE-CFE) Terpolymers. *Macromolecules* **2007**, *40*, 2371–2379.
47. Chu, B.; Zhou, X.; Ren, K.; Neese, B.; Lin, M.; Wang, Q.; Bauer, F.; Zhang, Q. M. A Dielectric Polymer with High Electric Energy Density and Fast Discharge Speed. *Science* **2006**, *313*, 334–336.
48. Barbosa, R.; Mendes, J. A.; Sencadas, V.; Mano, J. F.; Lanceros-Méndez, S. Chain Reorientation in β-PVDF Films upon Transverse Mechanical Deformation Studied by SEM and Dielectric Relaxation. *Ferroelectrics* **2003**, *294*, 73–83.
49. Ohigashi, H.; Akama, S.; Koga, K. Lamellar and Bulk Single Crystals Grown in Annealed Films of Vinylidene Fluoride and Trifluoroethylene Copolymers. *Jpn. J. Appl. Phys.* **1988**, *27*, 2144–2150.

50. Koga, K.; Ohigashi, H. Piezoelectricity and Related Properties of Vinylidene Fluoride and Trifluoroethylene Copolymers. *J. Appl. Phys.* **1986**, *59*, 2142–2150.
51. Zavala, G.; Fendler, J. H.; Trolier-Mckinstry, S. Characterization of Ferroelectric Lead Zirconate Titanate Films by Scanning Force Microscopy. *J. Appl. Phys.* **1997**, *81*, 7480–7491.
52. Kholkin, A. L.; Shvartsman, V. V.; Emelyanov, A. Y.; Poyato, R.; Calzada, M. L.; Pardo, L. Stress-Induced Suppression of Piezoelectric Properties in $PbTiO_3$:La Thin Films via Scanning Force Microscopy. *Appl. Phys. Lett.* **2003**, *82*, 2127–2129.
53. Zhang, Q. M.; Zhao, J.; Uchino, K.; Zheng, J. Change of the Weak-Field Properties of $Pb(ZrTi)O_3$ Piezoceramics with Compressive Uniaxial Stresses and Its Links to the Effect of Dopants on the Stability of the Polarizations in the Materials. *J. Mater. Res.* **1997**, *12*, 226–234.
54. Ishibashi, Y.; Iwata, M. Landau Theory of Phase Transition in Ferroelectric Vinylidene Fluoride/Trifluoroethylene Copolymer Single Crystals. *Jpn. J. Appl. Phys.* **2005**, *44*, 6624–6628.
55. Liu, Y. Y.; Yang, L.; Li, J. Y. Strain-Engineered Orthorhombic-Rhombohedral Phase Boundary in Epitaxial Bismuth Ferrite Films. *J. Appl. Phys.* **2013**, *113*, 183524.
56. Eliseev, E. A.; Kalinin, S. V.; Jesse, S.; Bravina, S. L.; Morozovska, A. N. Electromechanical Detection in Scanning Probe Microscopy: Tip Models and Materials Contrast. *J. Appl. Phys.* **2007**, *102*, 014109.